How to cite: *Angew. Chem. Int. Ed.* **2024**, *63*, e202406438
doi.org/10.1002/anie.202406438

Photosensitizers

A Tetracarbene Iron(II) Complex with a Long-lived Triplet Metal-to-Ligand Charge Transfer State due to a Triplet-Triplet Barrier

*Thomas Reuter, Dimitri Zorn, Robert Naumann, Jan Klett, Christoph Förster, and Katja Heinze**

Abstract: Mixed N-heterocyclic carbene (NHC) / pyridyl iron(II) complexes have attracted a great deal of attention recently because of their potential as photocatalysts and light sensitizers made from Earth-abundant elements. The most decisive challenge for their successful implementation is the lifetime of the lowest triplet metal-to-ligand charge transfer state (^{3}MLCT), which typically decays via a triplet metal-centered (^{3}MC) state back to the ground state. We reveal by variable-temperature ultrafast transient absorption spectroscopy that the tripodal iron(II) bis(pyridine) complex isomers ***trans***- and ***cis*-[Fe(pdmi)$_2$]$^{2+}$** with four NHC donors show ^{3}MLCT→^{3}MC population transfers with very different barriers and rationalize this by computational means. While ***trans*-[Fe(pdmi)$_2$]$^{2+}$** possesses an unobservable activation barrier, the cis isomer exhibits a barrier of 492 cm^{-1}, which leads to a nanosecond ^{3}MLCT lifetime at 77 K. The kinetic and quantum chemical data were analyzed in the context of semi-classical Marcus theory revealing a high reorganization energy and small electronic coupling between the two triplet states. This highlights the importance of detailed structural control and kinetic knowledge for the rational design of photosensitizers from first row transition metals such as iron.

1. Introduction

Controlling the interplay between charge transfer (CT) and metal-centered (MC) excited states constitutes an essential ingredient to the development of 3d metal complex luminophores and photoredox catalysts, in particular with iron as the most abundant transition metal.[1–4] While the photoactive metal-to-ligand charge transfer (MLCT) states are often well characterized by (ultrafast) optical transient absorption (TA) spectroscopy thanks to their characteristic absorption bands pertaining to a ligand radical anion[5] and an oxidized metal center, the largely photoinactive MC states are challenging to identify by TA spectroscopy. In selected cases, ultrafast X-ray spectroscopies at XFELs (X-Ray Free-Electron Lasers) can fill this knowledge gap provided that suitable model complexes for intermediate states are available.[6] Femtosecond transient mid-IR spectroscopy has been recently used to disentangle triplet and quintet metal centered states (^{3}MC and ^{5}MC) of iron(II) complexes.[7] The dynamics of the classical polypyridine complex **[Fe(bpy)$_3$]$^{2+}$** follows a sequential model ^{3}MLCT→^{3}MC→^{5}MC on a sub-picosecond time scale before decaying to the singlet ground state ^{1}GS on longer times scales (bpy = 2,2′-bipyridine, Figure 1).[6] The ^{5}MC→^{1}GS spin-crossover of **[Fe(bpy)$_3$]$^{2+}$** has been probed by variable-temperature (VT) TA spectroscopy by *McCusker* giving an activation barrier $E_a = 310$ cm^{-1} and a very small electronic coupling constant $H_{ab} = 4.3$ cm^{-1} due to the spin change of $\Delta S = 2$.[8] In polycarbene iron(II) complexes the ^{5}MC state is often too high in energy to be populated and hence the dynamics can be described by a

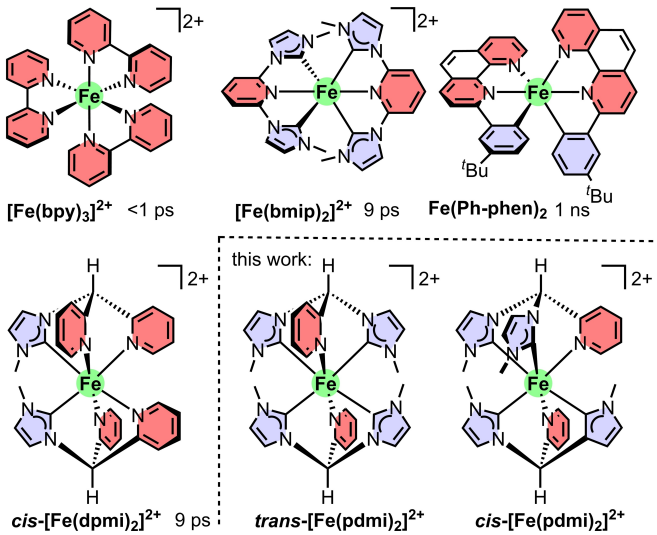

Figure 1. Molecular structures of selected pyridine iron(II) complexes with their ^{3}MLCT lifetimes at room temperature and the isomeric tetracarbene iron(II) complexes ***trans***- and ***cis*-[Fe(pdmi)$_2$]$^{2+}$** designed and examined in this work.

[*] T. Reuter, D. Zorn, Dr. R. Naumann, Dr. J. Klett, Dr. C. Förster, Prof. Dr. K. Heinze
Department of Chemistry
Johannes Gutenberg University Mainz
Duesbergweg 10–14, 55128 Mainz, Germany
E-mail: katja.heinze@uni-mainz.de

© 2024 The Authors. Angewandte Chemie International Edition published by Wiley-VCH GmbH. This is an open access article under the terms of the Creative Commons Attribution License, which permits use, distribution and reproduction in any medium, provided the original work is properly cited.

© 2024 The Authors. Angewandte Chemie International Edition published by Wiley-VCH GmbH

three-state model as ^{3}MLCT→^{3}MC→^{1}GS after an ultrafast intersystem crossing (ISC) from the ^{1}MLCT state. Yet, branching can occur from hot ^{3}MLCT or ^{1}MLCT states to the cold ^{3}MLCT and ^{3}MC states.[9,10] In *Wärnmark's* seminal tetracarbene photosensitizer **[Fe(bmip)$_2$]$^{2+}$** the ^{3}MLCT→^{3}MC population transfer occurs with a time constant of 9 ps[11] according to ultrafast X-ray spectroscopies (bmip = 2,6-bis(3-methyl-imidazole-1-ylidine)-pyridine, Figure 1).[12] VT-TA spectroscopic experiments, which do not rely on XFELs, were not yet performed for iron(II) complexes with extended lifetimes, such as polycarbene iron(II) complexes, to access the decisive ^{3}MLCT→^{3}MC barrier for the ^{3}MLCT lifetime, although this "*would be of highest interest*".[13]

The number of NHCs in polypyridine iron(II) complexes with meridional coordinating tridentate ligands contributes to the ^{3}MLCT lifetime enhancement,[14] implying that an additive ligand field,[15,16] which determines the ^{3}MC state energy, can be assumed in this series. Electron withdrawing substituents at the pyridine or replacement of the pyridine by electron-deficient pyrazine or pyrimidine boost the lifetime of derivatives of **[Fe(bmip)$_2$]$^{2+}$** to 26 ps and even 32 ps by lowering the MLCT state energies.[17,18] A tripodal coordination motif in ***cis*-[Fe(dpmi)$_2$]$^{2+}$** instead of the meridional motif achieves a 9 ps ^{3}MLCT lifetime already with two NHCs instead of four in **[Fe(bmip)$_2$]$^{2+}$** (dpmi = di(pyridine-2-yl)(3-methylimidazol-2-yl)methane, Figure 1).[19] Tris(bidentate) carbene/pyridine complexes [Fe(C^N)$_3$]$^{2+}$ possess ^{3}MLCT lifetimes of 3–20 ps with *facial* isomers featuring the longer lifetimes. This difference between *fac* and *mer* isomers shows that a simple additive ligand field is not a sufficient descriptor for the excited state dynamics.[20] Rather *trans* effects[21] might influence the excited state dynamics. The hexacarbene complex **[Fe(btz)$_3$]$^{2+}$** displays the highest ^{3}MLCT lifetime (528 ps) of a carbene iron(II) complex so far (btz = 3,3′-dimethyl-1,1′-bis(*p*-tolyl)-4,4′-bis(1,2,3-triazol-5-ylidene)).[22] *Dixon* and co-workers had computationally investigated the relative ^{3}MLCT/^{3}MC energy levels in iron(II) complexes with tridentate phenylbipyridine ligands. The ^{3}MC state is destabilized when *trans*-N–Fe–C arrangements dominate, i.e. not only the number, but also the coordination site of the phenyl σ-donor determines the ^{3}MC state energies.[23,24] This prediction was experimentally confirmed with the luminescent bis(cyclometalated) complex **Fe(Ph-phen)$_2$** with a ^{3}MLCT lifetime of 1 ns (H–Ph-phen = 9-phenylphenanthroline, Figure 1).[25]

Clearly, the number and position of NHCs/pyridines, the octahedricity (X–Fe–Y angles)[26–30] and the rigidity/flexibility[31,32] in the excited states play key roles for the (thermally activated) ^{3}MLCT to ^{3}MC internal conversion. However, the barrier and the electronic coupling between these triplet states decisive for the excited state dynamics are challenging to identify. *trans*-N–Fe–N coordination[23,24] with a rather weak average ligand field strength along this axis (z) will become the preferred Jahn–Teller axis in the lowest energy ^{3}MC state in NHC/pyridine iron(II) complexes. We hypothesize that the ^{3}MC state energy will be higher in the absence of an active N–Fe–N Jahn–Teller axis.

In this study, we probe the electronic and dynamic effects of the presence or absence of a weak ligand field axis by means of two designed iron(II) complex isomers with the same average [FeN$_2$C$_4$] ligand field spanned by two pyridines and four NHCs in a strictly octahedral geometry, but with different arrangements of the nitrogen donors, namely ***trans*-** and ***cis*-[Fe(pdmi)$_2$]$^{2+}$** (H$_2$pdmi = (2-pyridyl)di(3-methylimidazolium-1-yl)methane-bis(hexafluorophosphate); Figure 1).

2. Results and Discussion

2.1. Quantum Chemical Calculations

Geometries and energies of the singlet ground state (^{1}GS) and the lowest energy triplet and quintet states for both isomers ***trans*-** and ***cis*-[Fe(pdmi)$_2$]$^{2+}$** were calculated by quantum chemical methods on the density functional theory level (DFT, B3LYP functional, TZVP basis set, with dispersion and relativistic correction and continuum solvent model; Figures S1–S4; Tables S1–S4).

The key metrics of the iron(II) coordination in the optimized ^{1}GS and ^{3}MC states is depicted in Figure 2. The main changes involve the Fe–N bonds, which increase from ca. 2 Å in the ^{1}GS to 2.445 Å and to 2.518/2.175 Å in the ^{3}MC states of the *trans* and *cis* isomers, respectively. Energies of the lowest singlet, triplet and quintet states were calculated along the respective Fe–N elongation pathways (Figure 2). The first excited singlet and triplet states were estimated by time-dependent DFT (TDDFT) methods at the respective geometries and plotted in the potential energy diagrams (Figure 2). The ^{3}MLCT or ^{3}MC character of the triplet states was identified by inspection of the calculated spin densities.

For both isomers the high-spin state (^{5}MC) is higher in energy than the ^{3}MC state, which is typical for carbene iron(II) complexes,[14,17–19,33] but not for polypyridine iron(II) complexes.[26–30] At the Franck–Condon geometry, the ^{5}MC state of the *cis* isomer is higher than the MLCT states, while the ^{5}MC state of the *trans* isomer is closer to the MLCT states, although the $^{1/3}$MLCT states are likely calculated too high in energy. In contrast to the ^{1}MLCT states at the Franck–Condon geometry, which are delocalized over the iron center and all pyridines (Tables S3 and S4), the spin densities of the ^{3}MLCT states are confined to the iron center and a single pyridine (Figure 2). Hence, the energies of the relaxed ^{3}MLCT states of the pyridine iron(II) complexes are rather similar. At short Fe–N distances, the lowest triplet state possesses ^{3}MLCT character, while at larger distances the ^{3}MC state rapidly decreases in energy and the ^{3}MC character dominates the lowest triplet state. Consequently, the ^{3}MC state crosses the ^{3}MLCT state. Importantly, the optimized ^{3}MC state of ***cis*-[Fe(pdmi)$_2$]$^{2+}$** is at higher energy by 0.36 eV than the optimized ^{3}MC state of the *trans* isomer (Figure 2). The higher energy ^{3}MC state arises from the

© 2024 The Authors. Angewandte Chemie International Edition published by Wiley-VCH GmbH

15213773, 2024, 39, Downloaded from https://onlinelibrary.wiley.com/doi/10.1002/anie.202406438 by Universitätsbibliothek Mainz, Wiley Online Library on [28/04/2025]. See the Terms and Conditions (https://onlinelibrary.wiley.com/terms-and-conditions) on Wiley Online Library for rules of use; OA articles are governed by the applicable Creative Commons License

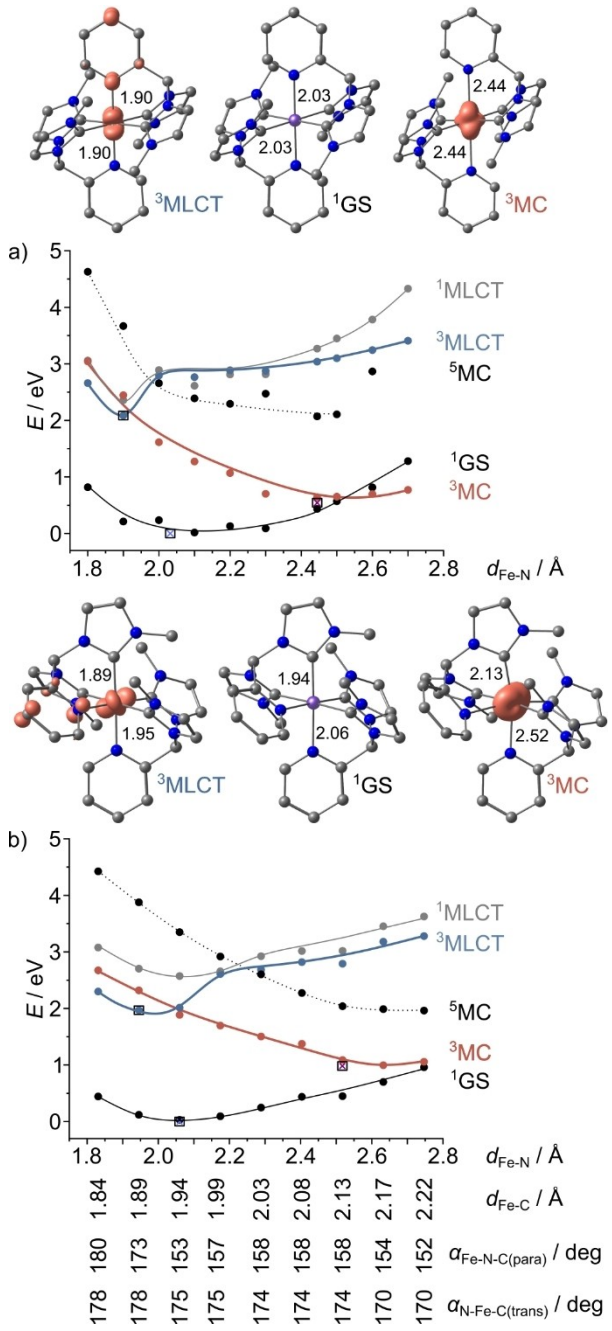

Figure 2. Schematic representation of the potential energy curves estimated by DFT/TDDFT methods of a) ***trans*-[Fe(pdmi)$_2$]$^{2+}$** along the symmetric Fe–N stretching mode and b) ***cis*-[Fe(pdmi)$_2$]$^{2+}$** along a single Fe–N stretching mode. The "diabatic" lines merely serve as a guide to the eye. Geometries with spin densities (orange, isosurface value 0.01 a.u.; H atoms omitted) of the ^{3}MC and ^{3}MLCT states are depicted at the indicated points ☒ with distances in Å.

presence of only *trans*-N–Fe–C and *trans*-C–Fe–C coordination and the absence of an "easy Jahn–Teller axis" with *trans*-N–Fe–N coordination similar to the computational predictions for cyclometalated complexes.[23,24] The ^{3}MC energy of the *trans* isomer rapidly decreases along the Jahn–Teller axis, while the ^{3}MC energy gradient is less steep for the *cis* isomer with a *trans*-N–Fe–C easy axis (Figure 2). This different gradient of the ^{3}MC energies along the Jahn–Teller axes shifts the ^{3}MLCT/^{3}MC crossing point to larger geometric distortions and suggests a higher barrier of the thermally activated ^{3}MLCT→^{3}MC internal conversion for ***cis*-[Fe(pdmi)$_2$]$^{2+}$**. These computational predictions will be elaborated experimentally in the following.

2.2. Syntheses, Structures and Redox Chemistry

The pro-ligand [H$_2$pdmi][PF$_6$]$_2$ was prepared from pyridine-2-carbaldehyde and 1,1-carbonyldiimidazole in 41 % overall yield (Figures S5–S6). Coordination of the tripodal ligand pdmi to iron(II) at −70 °C, chromatographic workup and recrystallization yielded **[Fe(pdmi)$_2$][PF$_6$]$_2$** as orange crystalline material as confirmed by ESI mass spectrometry and elemental analysis (Figure S7). HPLC analysis suggested the presence of *trans* and *cis* isomers in a 4:1 ratio (Figure S8). Preparative HPLC yielded pure ***trans*-[Fe(pdmi)$_2$][PF$_6$]$_2$** (Figures S9–S16). Due to low amount of *cis* isomer formed at −70 °C, a high temperature synthesis was developed to increase the proportion of the desired *cis* isomer. This isomer is slightly thermodynamically stabilized according to the DFT calculations with $\Delta G_{298K} = -5$ kJ mol^{-1}. Yet, higher temperature also favors NHC ligand decomposition. Gratifyingly, at 20 °C the *trans*:*cis* ratio increased to 1:2 (Figure S17). HPLC separation yielded pure ***cis*-[Fe(pdmi)$_2$][PF$_6$]$_2$** (Figures S18–S22). NMR and IR/Raman spectroscopic data of ***trans*-[Fe(pdmi)$_2$]$^{2+}$** and ***cis*-[Fe(pdmi)$_2$]$^{2+}$** are compatible with the proposed symmetries and the diamagnetic nature (low-spin) of the iron(II) complexes (Figures S10–S11, S14–S16, Figures S19–S24). The structures of the cations were confirmed by SC-XRD (Figures S25–S26).[34] The DFT calculations reproduce the high octahedricity, the Fe–N/C distances (Tables S1–S2) and the vibrational frequencies and intensities (Figures S23–S24).

Thanks to the strongly σ-donating carbene ligands, the iron(II) complexes are easily oxidized to the respective purple iron(III) complexes by spectroelectrochemistry or by using [NO][PF$_6$] (Figure S27–S30). The iron(III) complexes show characteristic CT absorption bands at 517/572 nm and 490/529/582/620(sh) nm for ***trans*-** and ***cis*-[Fe(pdmi)$_2$]$^{3+}$**, respectively (Figures S29–S30), similar to the 522/610 nm absorption bands of the bis(carbene) complex ***cis*-[Fe(dpmi)$_2$]$^{3+}$**.[19] The absorption bands of the iron(III) complexes will assist the interpretation of the TA data below.

2.3. Non-Radiative Decay: Steady-State and Time-Resolved Spectroscopy

Both iron(II) isomers display intense ^{1}MLCT absorption bands in the visible spectral region (Figure 3a, Figures S3–S4). The maxima appear at 521 and 471 nm (7430 and 8680 M^{-1}cm^{-1}) for ***trans*-** and ***cis*-[Fe(pdmi)$_2$]$^{2+}$**, respec-

© 2024 The Authors. Angewandte Chemie International Edition published by Wiley-VCH GmbH

15213773, 2024, 39, Downloaded from https://onlinelibrary.wiley.com/doi/10.1002/anie.202406438 by Universitätsbibliothek Mainz, Wiley Online Library on [28/04/2025]. See the Terms and Conditions (https://onlinelibrary.wiley.com/terms-and-conditions) on Wiley Online Library for rules of use; OA articles are governed by the applicable Creative Commons License

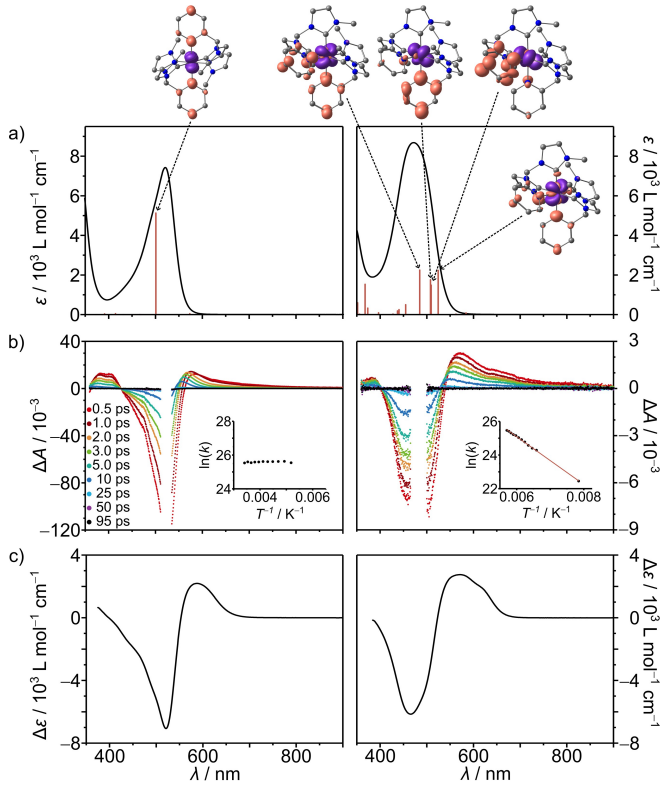

Figure 3. a) Absorption spectra of ***trans*-[Fe(pdmi)$_2$]$^{2+}$** (left) and ***cis*-[Fe(pdmi)$_2$]$^{2+}$** (right) in MeCN at 293 K. DFT calculated singlet transitions shown as sticks (bathochromically shifted by 3600 cm^{-1}). Selected difference densities at 0.006 a.u. (purple = electron density loss, orange = electron density gain; hydrogen atoms omitted). b) fs-TA spectra of ***trans*-[Fe(pdmi)$_2$]$^{2+}$** (left, λ_{exc} = 520 nm) and ***cis*-[Fe(pdmi)$_2$]$^{2+}$** (right, λ_{exc} = 470 nm) in MeOH/EtOH (2:3 *v*/*v*) at 293 K. ln(*k*) vs. 1/*T* plot in the insets, with $k = 1/\tau$ of the long-lived component. Arrhenius fit $k = e^{\left(-\frac{E_a}{k_B T}\right)}$ for ***cis*-[Fe(pdmi)$_2$]$^{2+}$** shown in red. c) Difference spectrum between ***trans*-[Fe(pdmi)$_2$]$^{3+}$** and ***trans*-[Fe(pdmi)$_2$]$^{2+}$** (left) and between ***cis*-[Fe(pdmi)$_2$]$^{3+}$** and ***cis*-[Fe(pdmi)$_2$]$^{2+}$** (right) at 293 K in MeCN.

tively, and are characterized by charge shifts from the iron center to the two pyridines (Figure 3a, top). According to TDDFT calculations and charge transfer number analyses (Tables S3–S4, Figures S3–S4), the sharper band of the *trans* complex is assigned to a single transition (Fe→py$_2$; calcd at 424 nm, with oscillator strength $f = 0.162$), while the broader band of the *cis* isomer is composed of four Fe→py$_2$ transitions at 413, 429, 430 and 441 nm with similar oscillator strengths ($f = 0.047$, 0.037, 0.031, 0.047). Hence, the TDDFT calculations nicely reproduce the experimental ^{1}MLCT band shape. According to the calculations, the *trans* and *cis* isomers exhibit additional weak low-energy transitions at 475/470/462/455 ($f = 0.00152/8.0\times10^{-9}/1.1\times10^{-8}/1.5\times10^{-8}$) and 483/468 nm ($f = 0.00185/0.00058$), respectively (Tables S3–S4). The presence of only weakly allowed low-energy ^{1}MLCT bands will be relevant for the discussion of the radiative decay below.

To probe the excited state dynamics, we employed VT ultrafast TA spectroscopy (Figures S31–S63). fs-TA spectra of both iron(II) complexes were recorded at 293 K in MeOH/EtOH (2:3 *v*/*v*) (Figure 3b, Figures S31–S32). In both cases, the ground state bleach (GSB) fits to the respective (negative) ^{1}MLCT absorption band suggesting only weak excited state absorptions (ESAs) in this spectral region (Figure 3). Low-energy ESA at 570/585 nm (hot, i.e. < 0.5 ps) and 555/545 nm (thermally relaxed) is apparent for the *trans*/*cis* isomers. These ESAs fit to the absorption bands of the respective iron(III) complexes (Figure 3c, Figures S29–S30). This match suggests an iron(III) character of the excited states supporting the MLCT nature as typically observed for NHC iron(II) complexes.[11,13,14,17–20,32,33] The ESAs around 400 nm can be assigned to the signature of pyridine radical anions with electron withdrawing substituents.[5] This fits to the MLCT assignment of this state.[35] The TDDFT calculated absorption bands of the ^{3}MLCT state matching with the TA spectra (Figures S62–S63) and the solvent dependence of the dynamics (Figures S31–S32, S60–S61) further confirm the ^{3}MLCT assignment. Consequently, the ^{3}MC→^{1}GS ISC occurs directly without a measureable barrier in both cases. The parallel ESA decay and GS recovery without accumulation of intermediate states confirm that only a single reaction dominates the dynamics in the ^{3}MLCT→^{3}MC→^{1}GS sequence. This is also suggested by the DFT calculations (Figure 2).

The ^{3}MLCT lifetimes of the *trans* and *cis* isomers at 293 K amount to $\tau_{293K}(trans) = 8.0/14.5$ ps and $\tau_{293K}(cis) = 8.6/15.2$ ps MeOH/EtOH (2:3 *v*/*v*) and MeCN, respectively (Figures S31–S32/S60–S61). Conversely, ^{3}MLCT lifetimes of a bis(cyanido) macrocyclic iron(II) complex are longer in MeOH than in MeCN, which might be explained by distinct Lewis acid/Lewis base interactions of the solvent with the coordinated cyanide.[31] The values for **[Fe(pdmi)$_2$]$^{2+}$** are similar to the 9 ps ^{3}MLCT lifetime of the bis(carbene) complex ***cis*-[Fe(dpmi)$_2$]$^{2+}$** in spite of the larger average ligand field imposed by four carbenes.[19] The different excited state dynamics of ***cis*-[Fe(pdmi)$_2$]$^{2+}$** as compared to the *trans* isomer reveals itself at lower temperature.

VT-TA spectroscopy for ***trans*-[Fe(pdmi)$_2$]$^{2+}$** between 293 and 193 K in fluid MeOH/EtOH solution shows no change in the lifetime, hence no activation barrier is observable (Figure 3b, left inset; Figures S33–S44). On the other hand, the VT-TA data of ***cis*-[Fe(pdmi)$_2$]$^{2+}$** reveal an Arrhenius-like behavior with an activation barrier $E_a = 492$ cm^{-1} and a pre-exponential factor $A = 1.35\times10^{12}$ s^{-1} (Figure 3b, right inset; Figures S45–S56). The larger barrier for the *cis* than for the *trans* isomer agrees with the DFT model (Figure 2). Expectedly, the barrier of ***cis*-[Fe(pdmi)$_2$]$^{2+}$** is much smaller than the barrier of 3800 cm^{-1} in the 4d metal complex **[Ru(bpy)$_3$]$^{2+}$** obtained by VT-luminescence lifetime measurements.[36–38] At 130 K in the viscous MeOH/EtOH mixture, the ^{3}MLCT lifetime of the *cis* isomer even increases to $\tau_{130K}(cis) = 177$ ps (Figure S57).

In the following, the Arrhenius data of ***cis*-[Fe(pdmi)$_2$]$^{2+}$** are discussed in the picture of semi-classical Marcus theory using harmonic potentials, although this

© 2024 The Authors. Angewandte Chemie International Edition published by Wiley-VCH GmbH

15213773, 2024, 39, Downloaded from https://onlinelibrary.wiley.com/doi/10.1002/anie.202406438 by Universitätsbibliothek Mainz, Wiley Online Library on [28/04/2025]. See the Terms and Conditions (https://onlinelibrary.wiley.com/terms-and-conditions) on Wiley Online Library for rules of use; OA articles are governed by the applicable Creative Commons License

might be an oversimplification in light of the anharmonic potentials calculated by DFT (Figure 2).[8] E_a is connected to the reorganization energy λ and the driving force ΔG_0 by eq. 1.[8]

$$E_a = \frac{(\Delta G_0 + \lambda)^2}{4\lambda} \quad (1)$$

$$A = \frac{2\pi}{\hbar}\frac{|H_{ab}^2|}{\sqrt{4\pi\lambda k_B T}} \quad (2)$$

As the driving force ΔG_0 is unknown experimentally, we estimate $\Delta G_0 = -(1.929–0.985)$ eV $= -7620 \pm 1000$ cm^{-1} from DFT derived energies of the ^{3}MLCT and ^{3}MC states (Figure 2). Solving the quadratic relationship for the reorganization energy gives $\lambda_1 = 12720 \pm 1250$ cm^{-1} and $\lambda_2 = 4570 \pm 750$ cm^{-1}, respectively. The lower value for the reorganization energy (λ_2) is discarded on the basis of the DFT calculations predicting a large energy difference (17290 cm^{-1}) between the ^{3}MC and ^{3}MLCT electronic structures at the ^{3}MC geometry. The substantial reorganization energy of $\lambda_1 = 12720$ cm^{-1} arises from the large displacement of the ^{3}MC potential curve along the Fe–N distortional axis (from ca. 2.0 to ca. 2.5 Å, Figure 2b). From the connection of the Arrhenius factor A with the electronic coupling H_{ab} by eq. 2, we estimate $H_{ab} = 81 \pm 6$ cm^{-1} for the ^{3}MLCT→^{3}MC internal conversion.

We discuss this unprecedented value of H_{ab} for a ^{3}MLCT to ^{3}MC reaction path of an iron(II) complex in comparison to the spin-crossover (^{5}MC→^{1}GS) process of **[Fe(bpy)$_3$]$^{2+}$** and M^{3+}/M^{2+} electron self-exchange reactions of iron and ruthenium complexes. Due to the second-order nature of the spin-crossover process, the electronic coupling between ^{5}MC and ^{1}GS is with $H_{ab} = 4.3$ cm^{-1} very small.[8] In the present case of ^{3}MLCT/^{3}MC coupling, no spin change is involved, so that a larger H_{ab} is plausible. The observed electronic coupling is somewhat larger than that for the **[Fe(H$_2$O)$_6$]$^{3+/2+}$** self-exchange reaction ($H_{ab} = 30$ cm^{-1} at an Fe···Fe distance of 6.36 Å),[39,40] but smaller than for $Ru^{3+/2+}$ self-exchange reactions at even larger distances ($H_{ab} = 100/145$ cm^{-1}, 10.5/13.3 Å).[39,41,42] Considering the short electron transfer distance for the ^{3}MLCT→^{3}MC transition, which can formally be described by a charge shift from the π* orbital of the pyridine to the $3d_{z2}$ orbital of iron[43] with a ring center to iron distance of ca. 3.3 Å, the value $H_{ab} = 81 \pm 6$ cm^{-1} appears rather small.

A closer look at the symmetries of the involved wave functions of the ^{3}MLCT→^{3}MC internal conversion and the spin densities (Figure 2b) of the ^{3}MLCT and ^{3}MC states is instructive (Figure 4). The pyridine π* and the iron $3d_{z2}$ orbital are close to orthogonal. This orthogonality should lead to a vanishing electronic coupling $H_{ab} \rightarrow 0$. However, in the ^{3}MC state, the pyridine is tilted with a Fe–N–C_{para} angle of 158° in addition to the Fe–N elongation and a small N–Fe–C(trans) angle compression from 178° to 174° (Figures 3 and 4).

The tilting of the ligand and the decrease of the N–Fe–C(trans) angle, which is already apparent at the ^{3}MLCT/^{3}MC crossing point (Figure 2b), leads to overlap of the pyridine π* and the iron $3d_{z2}$ orbitals as schematically illustrated in Figure 4. This overlap enables vibronic coupling[44–46] along this mode. In rigid matrices, tilting and hence the coupling might be reduced. Consequently, we measured the ^{3}MLCT lifetime of the *cis* isomer in a frozen MeOH/EtOH mixture at 77 K. Indeed, the ^{3}MLCT lifetime increases to the nanosecond range with $\tau_{77K}(cis) = 1.67$ ns (Figures S58–S59).

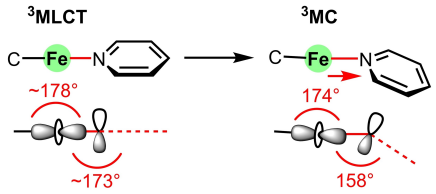

Figure 4. Schematic description of the modes determining the ^{3}MLCT→^{3}MC transition including the relevant orbitals, which affect the electronic coupling H_{ab}.

With the above interpretation of the ^{3}MLCT to ^{3}MC population transfer in the framework of Marcus theory, the parameters to raise the activation barrier for this detrimental process are the driving force ΔG_0, the reorganization energy λ and the electronic coupling H_{ab}. So far, the main efforts in the design of iron(II) photoactive complexes were devoted to lowering ΔG_0 by increasing the energy of the ^{3}MC and/or decreasing the energy of the ^{3}MLCT states. Here, we suggest λ and H_{ab} as additional decisive parameters. The reorganization energy λ is composed of inner-sphere and outer-sphere components λ_i and λ_o. The inner-sphere reorganization energy λ_i increases by a large nuclear displacement along a specific mode. However, large displacements also lower the energy of the relaxed ^{3}MC state, which raises ΔG_0. The outer-sphere reorganization energy λ_o should increase in polar solvents as the ^{3}MLCT and ^{3}MC states have large and small dipole moments, respectively. The DFT calculated change in dipole moment amounts to $\Delta\mu = 11$ D for ***cis*-[Fe(pdmi)$_2$]$^{2+}$**. Huge dipole moments have also been measured for the $^{1/3}$MLCT states of **[Fe(bpy)$_3$]$^{2+}$**.[43] Hence solvent polarity might be a useful parameter. However, polar solvents also stabilize the MLCT states, which counteracts the increase in λ_o. Furthermore solvent effects can even play subtle roles in transitions between MC states, e.g. in the ^{5}MC→^{1}GS spin-crossover.[47] These considerations on λ make straightforward predictions challenging.

2.4. Radiative Decay

The long ^{3}MLCT lifetime of ***cis*-[Fe(pdmi)$_2$]$^{2+}$** at 77 K prompted us to attempt luminescence measurements with MLCT excitation (450 nm cw laser; 450 and 470 nm Xe arc lamp; observation range 475–1600 nm) in frozen MeOH/EtOH solution and in the solid state at 77 K. However, no ^{3}MLCT luminescence band could be observed with our equipment.

© 2024 The Authors. Angewandte Chemie International Edition published by Wiley-VCH GmbH

15213773, 2024, 39, Downloaded from https://onlinelibrary.wiley.com/doi/10.1002/anie.202406438 by Universitätsbibliothek Mainz, Wiley Online Library on [28/04/2025]. See the Terms and Conditions (https://onlinelibrary.wiley.com/terms-and-conditions) on Wiley Online Library for rules of use; OA articles are governed by the applicable Creative Commons License

$$k_p(\tilde{T}_1^{\alpha}) = \frac{4}{3\hbar^4 c^3}(\Delta E_{TS})^3 \sum_{\gamma}^{x,y,z} \left| \sum_{m=1}^{\infty} \frac{\langle T_m^{\alpha}|H_{SO}|S_0\rangle}{E(S_0)-E(T_m)} \langle T_1^{\alpha}|M_{\gamma}|T_m^{\alpha}\rangle + \sum_{n=0}^{\infty} \frac{\langle S_n|H_{SO}|T_1^{\alpha}\rangle^*}{E(T_1)-E(S_n)} \langle S_n|M_{\gamma}|S_0\rangle \right|^2 \quad (3)$$

This raises the question why the phosphorescence rate $k_p(T_1 \rightarrow S_0)$ of ***cis*-[Fe(pdmi)$_2$]$^{2+}$** is so small that no luminescence is observed in spite of the nanosecond lifetime (with $T_1 = {}^3$MLCT and $S_0 = {}^1$GS). Phosphorescence rate constants k_p (eq. 3) rely on intensity borrowing of the T_1 state (^{3}MLCT) from S_m states (^{1}MLCT's), which are close in energy, i.e. with small $E(S_m) - E(T_1)$ energy differences. These singlet states should possess high transition dipole moments $\langle S_0|\sum_j e\vec{r}_j|S_m\rangle$ and a different orbital composition than the T_1 state to induce spin-orbit coupling $\langle S_m|\hat{H}_{SO}|T_{1,i}\rangle$.[44–46] Inspection of the lowest energy ^{1}MLCT transitions of ***cis*-[Fe(pdmi)$_2$]$^{2+}$** calculated by TDDFT (Table S4) reveals that the lowest energy ^{1}MLCT states, which are close in energy to the ^{3}MLCT state, possess only very small oscillator strengths $f < 0.0016$ and hence small transition dipole moments. Furthermore, their orbital composition is similar to that of the lowest energy ^{3}MLCT state, which prevents large spin-orbit coupling. Overall, the presence of these low-energy, low-intensity ^{1}MLCT states might explain the absence of luminescence of ***cis*-[Fe(pdmi)$_2$]$^{2+}$** in spite of the long ^{3}MLCT lifetime. Long lived but dark ^{3}MLCT states of iron(II) complexes had been reported before in a few cases, yet this discrepancy was not discussed before.[22,31]

3. Conclusion

For the tetracarbene pyridine iron(II) complex ***cis*-[Fe(pdmi)$_2$]$^{2+}$** variable temperature transient absorption (VT-TA) spectroscopic measurements revealed an activation barrier of 492 cm^{-1} for the ^{3}MLCT→^{3}MC internal conversion leading to a nanosecond ^{3}MLCT lifetime at 77 K. The so far essentially neglected parameter of the excited state decay of iron(II) sensitizers, the electronic coupling of the ^{3}MLCT and ^{3}MC states H_{ab}, has been estimated for the first time and an iron-pyridine bending mode is suggested to vibronically couple these triplet states. Our study demonstrates that VT-TA measurements in conjunction with DFT calculations can reveal important information of the excited state dynamics, which would have been missed with room temperature spectroscopic data only. Reducing H_{ab} might be a viable strategy to retard non-radiative decay of iron(II) sensitizers. This might be achieved by increasing the electron transfer distance in the ^{3}MLCT→^{3}MC conversion and by rigidification of the chromophore. With the new information at hand, we actively strive to achieve high ^{3}MLCT lifetimes of iron(II) sensitizers at higher temperature.

Supporting Information

The Supporting Information contains synthesis and separation procedures, experimental spectroscopic data and quantum chemical data (pdf) including Cartesian coordinates (xyz). The authors have cited additional references within the Supporting Information.[48–71]

Acknowledgements

The authors acknowledge Dr. Dieter Schollmeyer and Dr. Luca M. Carrella for collection of XRD data and Philipp Sikora for initial experiments concerning ligand synthesis. This work was supported by the Deutsche Forschungsgemeinschaft (Priority Program SPP 2102 "Light-controlled reactivity of metal complexes", HE 2778/14-2) and through grants INST 247/1018-1 FUGG and INST 247/1082-1 FUGG to KH. Parts of this research were conducted using the supercomputer Elwetritsch and advisory services offered by the RPTU Kaiserslautern-Landau (https://hpc.rz.rptu.de) which is a member of the AHRP. Open Access funding enabled and organized by Projekt DEAL.

Conflict of Interest

The authors declare no conflict of interest.

Data Availability Statement

The data that support the findings of this study are available in the supplementary material of this article.

Keywords: iron · carbene ligands · Marcus theory · pyridine ligands · transient absorption spectroscopy

[1] L. H. M. de Groot, A. Ilic, J. Schwarz, K. Wärnmark, *J. Am. Chem. Soc.* **2023**, *145*, 9369–9388.
[2] N. Sinha, O. S. Wenger, *J. Am. Chem. Soc.* **2023**, *145*, 4903–4920.
[3] C. Förster, K. Heinze, *Chem. Soc. Rev.* **2020**, *49*, 1057–1070.
[4] O. S. Wenger, *Chem. Eur. J.* **2019**, *25*, 6043–6052.
[5] V. Kalyanaraman, C. N. R. Rao, M. V. George, *J. Chem. Soc. B* **1971**, 2406–2409.
[6] K. S. Kjær, T. B. Van Driel, T. C. B. Harlang, K. Kunnus, E. Biasin, K. Ledbetter, R. W. Hartsock, M. E. Reinhard, S. Koroidov, L. Li, M. G. Laursen, F. B. Hansen, P. Vester, M. Christensen, K. Haldrup, M. M. Nielsen, A. O. Dohn, M. I. Pápai, K. B. Møller, P. Chabera, Y. Liu, H. Tatsuno, C. Timm, M. Jarenmark, J. Uhlig, V. Sundström, K. Wärnmark, P. Persson, Z. Németh, D. Sárosiné Szemes, E. Bajnóczi, G. Vankó, R. Alonso-Mori, J. M. Glownia, S. Nelson, M. Sikorski, D. Sokaras, S. E. Canton, H. T. Lemke, K. J. Gaffney, *Chem. Sci.* **2019**, *10*, 5749–5760.
[7] C. Zahn, M. Pastore, J. L. P. Lustres, P. C. Gros, S. Haacke, K. Heyne, *J. Am. Chem. Soc.* **2024**, *146*, 9347–9355.
[8] M. C. Carey, S. L. Adelman, J. K. McCusker, *Chem. Sci.* **2019**, *10*, 134–144.

© 2024 The Authors. Angewandte Chemie International Edition published by Wiley-VCH GmbH

15213773, 2024, 39, Downloaded from https://onlinelibrary.wiley.com/doi/10.1002/anie.202406438 by Universitätsbibliothek Mainz, Wiley Online Library on [28/04/2025]. See the Terms and Conditions (https://onlinelibrary.wiley.com/terms-and-conditions) on Wiley Online Library for rules of use; OA articles are governed by the applicable Creative Commons License

[9] H. Tatsuno, K. S. Kjær, K. Kunnus, T. C. B. Harlang, C. Timm, M. Guo, P. Chàbera, L. A. Fredin, R. W. Hartsock, M. E. Reinhard, S. Koroidov, L. Li, A. A. Cordones, O. Gordivska, O. Prakash, Y. Liu, M. G. Laursen, E. Biasin, F. B. Hansen, P. Vester, M. Christensen, K. Haldrup, Z. Németh, D. Sárosiné Szemes, P. Bajnlczi, G. Vankl, T. B. Van Driel, R. Alonso-Mori, J. M. Glownia, S. Nelson, M. Sikorski, H. T. Lemke, D. Sokaras, S. E. Canton, A. O. Dohn, K. B. Møller, M. M. Nielsen, K. J. Gaffney, K. Wärnmark, V. Sundström, P. Persson, J. Uhlig, *Angew. Chem. Int. Ed.* **2020**, *59*, 364–372.

[10] F. Hainer, N. Alagna, A. Reddy Marri, T. J. Penfold, P. C. Gros, S. Haacke, T. Buckup, *J. Phys. Chem. Lett.* **2021**, *12*, 8560–8565.

[11] Y. Liu, T. Harlang, S. E. Canton, P. Chábera, K. Suárez-Alcántara, A. Fleckhaus, D. A. Vithanage, E. Göransson, A. Corani, R. Lomoth, V. Sundström, K. Wärnmark, *Chem. Commun.* **2013**, *49*, 6412–6414.

[12] K. Kunnus, M. Vacher, T. C. B. Harlang, K. S. Kjær, K. Haldrup, E. Biasin, T. B. van Driel, M. Pápai, P. Chabera, Y. Liu, H. Tatsuno, C. Timm, E. Källman, M. Delcey, R. W. Hartsock, M. E. Reinhard, S. Koroidov, M. G. Laursen, F. B. Hansen, P. Vester, M. Christensen, L. Sandberg, Z. Németh, D. S. Szemes, É. Bajnóczi, R. Alonso-Mori, J. M. Glownia, S. Nelson, M. Sikorski, D. Sokaras, H. T. Lemke, S. E. Canton, K. B. Møller, M. M. Nielsen, G. Vankó, K. Wärnmark, V. Sundström, P. Persson, M. Lundberg, J. Uhlig, K. J. Gaffney, *Nat. Commun.* **2020**, *11*, 634.

[13] C. Cebrián, M. Pastore, A. Monari, X. Assfeld, P. C. Gros, S. Haacke, *ChemPhysChem* **2022**, *23*, e202100659.

[14] P. Zimmer, L. Burkhardt, A. Friedrich, J. Steube, A. Neuba, R. Schepper, P. Müller, U. Flörke, M. Huber, S. Lochbrunner, M. Bauer, *Inorg. Chem.* **2018**, *57*, 360–373.

[15] R. J. Deeth, D. L. Foulis, B. J. Williams-Hubbard, *Dalton Trans.* **2003**, 3949–3955.

[16] J. Glerup, O. Mønsted, C. E. Schäfer, *Inorg. Chem.* **1976**, *15*, 1399–1407.

[17] L. Liu, T. Duchanois, T. Etienne, A. Monari, M. Beley, X. Assfeld, S. Haacke, P. C. Gros, *Phys. Chem. Chem. Phys.* **2016**, *18*, 12550–12556.

[18] M. Darari, E. Domenichini, A. Francés-Monerris, C. Cebrián, K. Magra, M. Beley, M. Pastore, A. Monari, X. Assfeld, S. Haacke, P. C. Gros, *Dalton Trans.* **2019**, *48*, 10915–10926.

[19] T. Reuter, A. Kruse, R. Schoch, S. Lochbrunner, M. Bauer, K. Heinze, *Chem. Commun.* **2021**, *57*, 7541–7544.

[20] K. Magra, E. Domenichini, A. Francés-Monerris, C. Cebrián, M. Beley, M. Darari, M. Pastore, A. Monari, X. Assfeld, S. Haacke, P. C. Gros, *Inorg. Chem.* **2019**, *58*, 5069–5081.

[21] B. J. Coe, S. J. Glenwright, *Coord. Chem. Rev.* **2000**, *203*, 5–80.

[22] P. Chábera, K. S. Kjaer, O. Prakash, A. Honarfar, Y. Liu, L. A. Fredin, T. C. B. Harlang, S. Lidin, J. Uhlig, V. Sundström, R. Lomoth, P. Persson, K. Wärnmark, *J. Phys. Chem. Lett.* **2018**, *9*, 459–463.

[23] I. M. Dixon, S. Khan, F. Alary, M. Boggio-Pasqua, J.-L. Heully, *Dalton Trans.* **2015**, *44*, 13498–13503.

[24] I. M. Dixon, F. Alary, M. Boggio-Pasqua, J.-L. Heully, *Dalton Trans.* **2014**, *43*, 15898–15905.

[25] W. Leis, M. A. Argüello Cordero, S. Lochbrunner, H. Schubert, A. Berkefeld, *J. Am. Chem. Soc.* **2022**, *144*, 1169–1173.

[26] L. L. Jamula, A. M. Brown, D. Guo, J. K. McCusker, *Inorg. Chem.* **2014**, *53*, 15–17.

[27] A. K. C. Mengel, C. Förster, A. Breivogel, K. Mack, J. R. Ochsmann, F. Laquai, V. Ksenofontov, K. Heinze, *Chem. Eur. J.* **2015**, *21*, 704–714.

[28] A. K. C. Mengel, C. Bissinger, M. Dorn, O. Back, C. Förster, K. Heinze, *Chem. Eur. J.* **2017**, *23*, 7920–7931.

[29] A. Britz, W. Gawelda, T. A. Assefa, L. L. Jamula, J. T. Yarranton, A. Galler, D. Khakhulin, M. Diez, M. Harder, G. Doumy, A. M. March, É. Bajnóczi, Z. Németh, M. Pápai, E. Rozsályi, D. Sárosiné Szemes, H. Cho, S. Mukherjee, C. Liu, T. K. Kim, R. W. Schoenlein, S. H. Southworth, L. Young, E. Jakubikova, N. Huse, G. Vankó, C. Bressler, J. K. McCusker, *Inorg. Chem.* **2019**, *58*, 9341–9350.

[30] J. Moll, R. Naumann, L. Sorge, C. Förster, N. Gessner, L. Burkhardt, N. Ugur, P. Nuernberger, W. Seidel, C. Ramanan, M. Bauer, K. Heinze, *Chem. Eur. J.* **2022**, *28*, e202201858.

[31] J. T. Malme, R. A. Clendening, R. Ash, T. Curry, T. Ren, J. Vura-Weis, *J. Am. Chem. Soc.* **2023**, *145*, 6029–6034.

[32] M. Darari, A. Francés-Monerris, B. Marekha, A. Doudouh, E. Wenger, A. Monari, S. Haacke, P. C. Gros, *Molecules* **2020**, *25*, 5991.

[33] L. Lindh, P. Chábera, N. W. Rosemann, J. Uhlig, K. Wärnmark, A. Yartsev, V. Sundström, P. Persson, *Catalysts* **2020**, *10*, 315.

[34] Deposition numbers 2339759 (for ***trans*-[Fe(pdmi)$_2$][PF$_6$]$_2$**), and 2339759 (for ***cis*-[Fe(pdmi)$_2$][PF$_6$]$_2$**) contain the supplementary crystallographic data for this paper. These data are provided free of charge by the joint Cambridge Crystallographic Data Centre and Fachinformationszentrum Karlsruhe Access Structures service.

[35] A. M. Brown, C. E. McCusker, J. K. McCusker, *Dalton Trans.* **2014**, *43*, 17635–17646.

[36] D. Hernández-Castillo, R. E. P. Nau, M.-A. Schmid, S. Tschierlei, S. Rau, L. González, *Angew. Chem. Int. Ed.* **2023**, *62*, e202308803.

[37] J. Van Houten, R. J. Watts, *J. Am. Chem. Soc.* **1976**, *98*, 4853–4858.

[38] J. V. Caspar, T. J. Meyer, *J. Am. Chem. Soc.* **1983**, *105*, 5583–5590.

[39] E. J. Piechota, G. J. Meyer, *J. Chem. Educ.* **2019**, *96*, 2450–2466.

[40] M. D. Newton, *Int. J. Quantum Chem.* **1980**, *18*, 363–391.

[41] J. E. Sutton, H. Taube, *Inorg. Chem.* **1981**, *20*, 3125–3134.

[42] C. Patoux, J.-P. Launay, M. Beley, S. Chodorowski-Kimmes, J.-P. Collin, S. James, J.-P. Sauvage, *J. Am. Chem. Soc.* **1998**, *120*, 3717–3725.

[43] A. B. Maurer, G. J. Meyer, *J. Am. Chem. Soc.* **2020**, *142*, 6847–6851.

[44] a) T. J. Penfold, E. Gindensperger, C. Daniel, C. M. Marian, *Chem. Rev.* **2018**, *118*, 6975–7025; b) A. Steffen, B. Hupp, in *Comprehensive Coordination Chemistry III* (Eds. E. C. Constable, G. Parkin, L. Que Jr), Elsevier **2021**, pp. 466–502.

[45] G. Baryshnikov, B. Minaev, H. Ågren, *Chem. Rev.* **2017**, *117*, 6500–6537.

[46] B. Minaev, G. Baryshnikov, H. Agren, *Phys. Chem. Chem. Phys.* **2014**, *16*, 1719–1758.

[47] J. N. Miller, J. K. McCusker, *Chem. Sci.* **2020**, *11*, 5191–5204.

[48] C. Müller, T. Pascher, A. Eriksson, P. Chabera, J. Uhlig, *J. Phys. Chem. A* **2022**, *126*, 4087–4099.

[49] F. Neese, *WIREs Comput. Mol. Sci.* **2018**, *8*, e1327.

[50] A. D. Becke, *J. Chem. Phys.* **1993**, *98*, 5648–5652.

[51] C. Lee, W. Yang, R. G. Parr, *Phys. Rev. B* **1988**, *37*, 785–789.

[52] B. Miehlich, A. Savin, H. Stoll, H. Preuss, *Chem. Phys. Lett.* **1989**, *157*, 200–206.

[53] D. A. Pantazis, X.-Y. Chen, C. R. Landis, F. Neese, *J. Chem. Theory Comput.* **2008**, *4*, 908–919.

[54] F. Weigend, R. Ahlrichs, *Phys. Chem. Chem. Phys.* **2005**, *7*, 3297–3305.

[55] F. Neese, F. Wennmohs, A. Hansen, U. Becker, *Chem. Phys.* **2009**, *356*, 98–109.

[56] R. Izsák, F. Neese, *J. Chem. Phys.* **2011**, *135*, 144105.

[57] S. Miertuš, E. Scrocco, J. Tomasi, *Chem. Phys.* **1981**, *55*, 117–129.

[58] V. Barone, M. Cossi, *J. Phys. Chem. A* **1998**, *102*, 1995–2001.

© 2024 The Authors. Angewandte Chemie International Edition published by Wiley-VCH GmbH

15213773, 2024, 39, Downloaded from https://onlinelibrary.wiley.com/doi/10.1002/anie.202406438 by Universitätsbibliothek Mainz, Wiley Online Library on [28/04/2025]. See the Terms and Conditions (https://onlinelibrary.wiley.com/terms-and-conditions) on Wiley Online Library for rules of use; OA articles are governed by the applicable Creative Commons License

[59] S. Grimme, J. Antony, S. Ehrlich, H. Krieg, *J. Chem. Phys.* **2010**, *132*, 154104.
[60] S. Grimme, S. Ehrlich, L. Goerigk, *J. Comput. Chem.* **2011**, *32*, 1456–1465.
[61] S. Mai, F. Plasser, J. Dorn, M. Fumanal, C. Daniel, L. González, *Coord. Chem. Rev.* **2018**, *361*, 74–97.
[62] F. Plasser, Theodore 2.0, http://theodore-qc.sourceforge.net.
[63] STOE & Cie, X-Area, STOE & Cie GmbH, Darmstadt, Germany.
[64] R. H. Blessing, *Acta Crystallogr. Sect. A* **1995**, *51*, 33–38.
[65] A. L. Spek, *Acta Crystallogr. Sect. D* **2009**, *65*, 148–155.
[66] J. Koziskova, F. Hahn, J. Richter, J. Kožíšek, *Acta Chim. Slov.* **2016**, *9*, 136–140.
[67] STOE & Cie, X-Area LANA, STOE & Cie GmbH, Darmstadt, Germany.
[68] G. M. Sheldrick, *Acta Crystallogr. Sect. A* **2015**, *71*, 3–8.
[69] G. M. Sheldrick, *Acta Crystallogr. Sect. C* **2015**, *71*, 3–8.
[70] G. M. Sheldrick, *Acta Crystallogr. Sect. A* **2008**, *64*, 112–122.
[71] C. B. Hübschle, G. M. Sheldrick, B. Dittrich, *J. Appl. Crystallogr.* **2011**, *44*, 1281–1284.

Manuscript received: April 5, 2024
Accepted manuscript online: July 1, 2024
Version of record online: August 23, 2024

© 2024 The Authors. Angewandte Chemie International Edition published by Wiley-VCH GmbH

15213773, 2024, 39, Downloaded from https://onlinelibrary.wiley.com/doi/10.1002/anie.202406438 by Universitätsbibliothek Mainz, Wiley Online Library on [28/04/2025]. See the Terms and Conditions (https://onlinelibrary.wiley.com/terms-and-conditions) on Wiley Online Library for rules of use; OA articles are governed by the applicable Creative Commons License